



**Plasma-Enhanced Atomic-Layer-Deposited Gallium Nitride
as an Electron Transport Layer for Planar Perovskite Solar
Cells**

Journal:	<i>Journal of Materials Chemistry A</i>
Manuscript ID	TA-ART-08-2019-008929.R1
Article Type:	Paper
Date Submitted by the Author:	10-Oct-2019
Complete List of Authors:	<p>Wei, Huiyun; University of Science and Technology Beijing, School of Mathematics and Physics</p> <p>Wu, Jionghua; Institute of Physics, Chinese Academy of Sciences, Beijing National Laboratory for Condensed Matter Physics</p> <p>Qiu, Peng; University of Science and Technology Beijing</p> <p>Liu, Sanjie; University of Science and Technology Beijing, School of Mathematics and Physics</p> <p>He, Yingfeng; University of Science and Technology Beijing, School of Mathematics and Physics</p> <p>Peng, Mingzeng; University of Science and Technology Beijing, School of Mathematics and Physics</p> <p>Li, Dongmei; Institute of Physics, Chinese Academy of Sciences, Beijing National Laboratory for Condensed Matter Physics</p> <p>Meng, Qingbo; Institute of Physics, Chinese Academy of Sciences, Beijing National Laboratory for Condensed Matter Physics</p> <p>Zaera, Francisco; University of California, Chemistry</p> <p>Zheng, Xinhe; University of Science and Technology Beijing, School of Mathematics and Physics</p>

ARTICLE

Plasma-Enhanced Atomic-Layer-Deposited Gallium Nitride as an Electron Transport Layer for Planar Perovskite Solar Cells

Received 00th January 20xx,
Accepted 00th January 20xx

DOI: 10.1039/x0xx00000x

Huiyun Wei,^a Jionghua Wu,^{b,c} Peng Qiu,^a Sanjie Liu,^a Yingfeng He,^a Mingzeng Peng,^a Dongmei Li,^{b,c} Qingbo Meng,^{*b,c} Francisco Zaera,^d and Xinhe Zheng^{*a}

Low-temperature deposited gallium nitride (GaN) thin-films have been introduced into planar perovskite solar cells (PSCs) as electron transport layers (ETLs) for the first time. Compact and amorphous n-type GaN layers were uniformly coated on fluorine-doped tin oxide (FTO) glass substrates via plasma-enhanced atomic layer deposition (PEALD) technology, in which an optimized deposition temperature of 280°C was identified and adopted. As-prepared GaN thin-films were subsequently employed to fabricate planar PSCs with the device configuration FTO/GaN/perovskite/spiro-OMeTAD/Au. Interestingly, although 0.59 eV of conduction-band-minimum (CBM) mismatch is found at the interface of 50-PEALD-cycle GaN/perovskite, significantly enhanced device efficiency from 10.38% to 15.18% has also been achieved relative to the ETL-free PSCs. Meanwhile, the current-voltage hysteresis and device stability of GaN-based PSCs can be remarkably improved. It is found that the GaN layer can promote the electron extraction and reduce recombination at the FTO/perovskite interface. This work demonstrates the feasibility and potential of GaN films as ETLs in planar PSCs.

Introduction

Perovskite solar cells (PSCs) show tremendous potential due to low-cost processing methods and excellent optoelectronic properties of perovskite materials. The latest certified efficiency for PSCs has reached values up to 25.2% within only few years of efforts by developing more efficient materials and structures, as well as deep understanding carrier dynamics.¹⁻¹⁰ However, some issues are still needed to be urgently solved, such as hysteresis and long-term stability, which are related to the imperfect carrier transport and interfacial contact. Generally, n-i-p PSCs can be typically fabricated in either mesoporous or planar configurations based on electron transport layers (ETLs), but both configurations consist of a transparent conducting oxide (FTO or ITO), a mesoporous or planar ETL, a perovskite light absorber, a hole transport layer (HTL) and an electrode (Au, Ag, carbon, etc.). Among these, the ETL is of crucial importance to accelerate electron extraction, transportation and collection

from the perovskite layer to the transparent electrode as well as to restrain the unfavourable interfacial charge recombination.¹¹⁻¹³ General requirements for ETLs in PSCs are considered to include the following: (i) high electron mobility for fast charge transport and good electrical conductivity for minimal series resistance (R_s); (ii) favourable energy level alignment with the perovskite layer for fast electron extraction and hole blocking; and (iii) a pin-hole-free structure to avoid direct contact between hole-transportation and the transparent electrode.^{14, 15} Although fast electron extraction and injection have been achieved for the most common TiO₂ ETL, it still has drawbacks such as relatively low electron mobility and poor photostability. Moreover, a high-temperature sintering (400-500°C) is usually required for those TiO₂ ETLs.^{16, 17} Therefore, other inorganic ETLs such as SnO₂ and ZnO, as well as organic ETLs, such as fullerene and its derivatives, have also been studied to replace TiO₂.^{18, 19} However, to achieve higher photovoltaic performance, efforts are still essential to constantly explore new materials and technology for the ETLs in PSCs.

Gallium nitride (GaN) is a direct-gap semiconductor with a bulk bandgap of 3.4 eV (Wurtzite crystal) similar to the metal oxides (TiO₂, ZnO, SnO₂, etc.),^{20, 21} which is a promising ETL candidate for PSCs due to its merits of good transparency, chemical stability, and high theoretical electron mobility (up to ~1000 cm² V⁻¹ s⁻¹ at 300 K).^{22, 23} So far, GaN has been applied into high electron mobility transistors, InGaN based solar cells and photodetectors.²⁴ However, to the best of our knowledge, only Alex Zettl et al reported a type of GaN ETL-based PSCs, in which GaN ETLs were prepared through a relatively

^aSchool of Mathematics and Physics, Beijing Key Laboratory for Magneto-Photoelectrical Composite and Interface Science, University of Science and Technology Beijing, Beijing 100083, China. E-mail: xinhezhen@ustb.edu.cn

^bKey Laboratory for Renewable Energy (CAS), Beijing Key Laboratory for New Energy Materials and Devices, Beijing National Laboratory for Condensed Matter Physics, Institute of Physics, Chinese Academy of Science, Beijing 100190, China. qbmeng@iphy.ac.cn

^cSchool of Physical Sciences, University of Chinese Academy of Sciences, Beijing 100049, China.

^dDepartment of Chemistry and UCR Centre of Catalysis, University of California, Riverside, CA 92521, USA.

†Electronic Supplementary Information (ESI) available: HRTEM image of GaN/Si(100) sample; Plots of $(\alpha hv)^2$ versus $h\nu$; XPS spectra; contact angle measurement. See DOI: 10.1039/x0xx00000x

complicated treatment for the commercial GaN on Si wafer.²⁵ GaN films are normally deposited on SiC, sapphire or crystalline silicon (c-Si) substrates by metal organic chemical vapor deposition (MOCVD) and molecular beam epitaxy (MBE).^{26, 27} Although GaN epitaxial films with high electron mobilities have been achieved by MOCVD or MBE, up to 800°C deposition temperatures restricts their application in the solar cells, far beyond the tolerable temperature of the frequently-used transparent electrodes (FTO or ITO). Therefore, exploring alternative low-temperature deposition methods for high quality GaN films on FTO or ITO substrates may open new opportunities for their use in solar cells.

So far, deposition of GaN films at the temperature range of 300-600°C has been achieved by pulsed laser deposition (PLD) and electron cyclotron resonance plasma enhanced MOCVD technology.^{28, 29} Besides, GaN films have also been deposited by RF-magnetron sputtering below 150°C.³⁰ Plasma-enhanced atomic layer deposition (PEALD) is a typically low-temperature deposition technology. Besides, PEALD offers unique advantages such as high control on film uniformity, conformality, and sub-nanometre thickness due to its self-limiting growth mechanism involved, typically, it can significantly lower GaN growth temperature below 300°C.³¹⁻³³ However, the quality of GaN thin films obtained by this way is relatively poor, with significantly reduced electric conductivity and mobility comparing to those prepared by MBE or MOCVD. In previous studies, Ozgit-Akgun et al deposited GaN thin films at 100-500°C by PEALD, and proved that a self-limiting ALD mode was feasible in the temperature range between 185 and 385°C.³⁴ Shih et al prepared GaN thin film on Si (100) substrates by remote plasma ALD, and obtained GaN films with uniform and almost atomic flat surfaces at 200-500°C.³⁵ In our previous work, GaN thin films were grown on a Si (100) substrate by PEALD at the temperatures of 200-350°C. We found that the crystalline quality can be improved by increasing deposition temperatures, that is, a ~18 nm-thick amorphous layer was formed by following a polycrystalline layer upon GaN deposition at 350°C.³⁶ Obviously, these researches provide the possibility for the growth of GaN films on FTO substrates, even though thin films properties are related to the underlying substrate.

Here, a kind of low-temperature deposited GaN thin films on FTO substrates has been obtained via PEALD with a preliminary optimized deposition temperature of 280°C. The effect of deposition parameters on the morphology, composition and photoelectric properties of the GaN thin films is systematically investigated. Subsequently, PEALD-prepared GaN is incorporated into planar PSCs by assembling a FTO/GaN/perovskite/spiro-OMeTAD/Au configuration. The effect of GaN thickness on interfacial electron transport, charge recombination and photovoltaic performance in planar PSCs was carefully evaluated. The results show that a device with a 50-PEALD-cycle GaN ETL can reach an efficiency of 15.18%, much higher than the 10.38% of ETL-free PSCs. This work shows the feasibility of using nitrides as ETLs in PSCs.

Further work is underway to evaluate the potential of using doping to improve the GaN electronic mobility and to pattern GaN surfaces to improve the quality of perovskite films.

Results and discussion

GaN films used here are deposited on FTO substrates at an optimized temperature of 280°C by using triethylgallium (TEG) as the Ga precursor and Ar/N₂/H₂ (1:3:6) plasma as the N source. The specific PEALD-GaN deposition process is illustrated schematically in Fig. 1, a complete ALD cycle consists of a TEG dose of 0.5 s and an Ar purge of 30 s followed by a plasma exposure of 30 s and reaction time of 45 s and an Ar purge of 30 s. A Si (100)/GaN sample was prepared under the same conditions as reference, because the FTO glass substrate is too fragile to ion milling during sample preparation for transmission electron microscopy (TEM) measurement. In general, higher quality GaN thin films can be obtained more easily on c-Si substrates than on rougher FTO glass. According to the high-resolution TEM image in Fig. S1, ~18 nm-thick GaN layer obtained on the Si (100) substrate is still amorphous, it is thus inferred that the GaN grown on FTO is also amorphous.

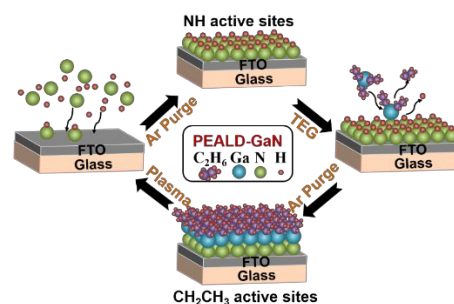


Fig. 1 Schematics of the PEALD deposition process used for the growth of GaN thin films.

The thickness of the GaN film depends on the number of PEALD cycles, a deposition rate (growth per cycle, GPC) of ~1.0 Å/cycle was determined by an ellipsometry. Here, for ease of characterization, a relatively thick GaN layer with 200 PEALD cycles (~19 nm-thick) is selected as representative to study the morphology, composition, and optical absorption. Fig. 2a and c show AFM images of the blank FTO glass and of the FTO/GaN sample, respectively, whereas Fig. 2b and d correspond to the complementary SEM images. It can be seen that the GaN layer uniformly covers the FTO crystals surfaces and smooths the sharp FTO crystal edges, as a result, the root-mean-square (RMS) roughness of FTO surface is decreased from 16.6 nm to 15.5 nm. Similar phenomenon has also been reported in the literatures for metal oxides grown on FTO glass by ALD.³⁷

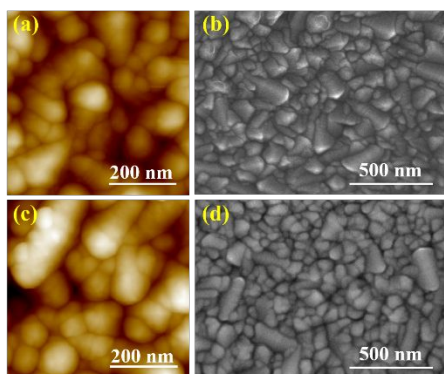


Fig. 2 The AFM and SEM images of blank FTO glass (a, b) and of a 200-PEALD-cycle GaN film grown on FTO glass (c, d), respectively.

UV-vis absorption spectra for the 200-PEALD-cycle GaN film on FTO glass is given in Fig. 3a. As a contrast, an obviously thinner GaN films (50 PEALD cycles) is also measured to determine the effect of GaN thickness on the absorption property. Two peaks are found in these two samples, the peak located at 325 nm is attributed to the absorption peak of GaN related to the bandgap.³⁸ The absorption peak is red-shifted from 325 to 350 nm when the film thickness is increased from 50 to 200 PEALD cycles, however, its intensity decreases instead. A thicker GaN film tends to have less dislocation densities due to the thickness dependent inter-diffusion effects at the interface of GaN/substrates.³⁹ Thus, the longer-wavelength peak could be a defect-related peak. Relationship of $(\alpha h\nu)^{1/2}$ versus $h\nu$ (where α is optical absorption coefficient, $h\nu$ is photon energy) is plotted in Fig. S2 to estimate their bandgap values. Bandgap values of 3.62 eV and 3.71 eV were calculated for the 200-PEALD-cycle and 50-PEALD-cycle GaN films, respectively. Besides, from the X-ray diffraction (XRD) results shown in Fig. 3b, poor crystallinity for the 200-PEALD-cycle GaN film is found. However, this situation could be improved for the obviously thicker 750-PEALD-cycle GaN film, which is similar to above TEM analysis for the GaN/Si sample.

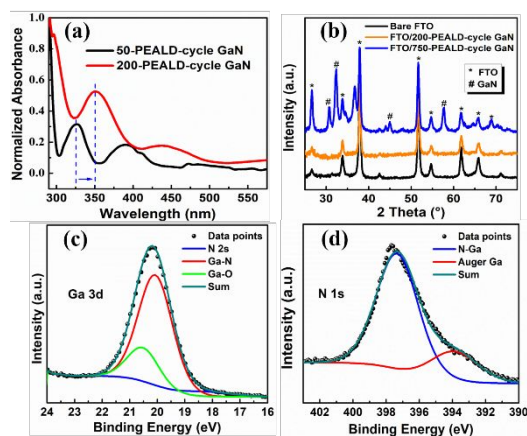


Fig. 3 (a) UV-vis absorption spectrum from 50-PEALD-cycle (black trace) and 200-PEALD-cycle (red) GaN/FTO films. (b) XRD spectra from bare FTO glass (black trace), FTO/200-PEALD-cycle GaN (yellow), and FTO/750-PEALD-cycle GaN (blue). (c) Ga 3d and (d) N 1s XPS spectra from the 200-PEALD-cycle GaN thin film.

The bonding states of the 200-PEALD-cycle GaN thin film are analyzed by XPS, as shown in Figs. 3(c, d) and S3. The N 1s XPS peak is deconvoluted into two peaks at 397.3 and 393.9 eV, which are

assigned to N-Ga and Auger Ga, respectively. The Ga 3d XPS peak is also deconvoluted into two components at 20.1 and 20.6 eV corresponding to Ga-N and Ga-O bonds (Fig. 3d). Further quantitative analysis of the XPS measurements reveals that the GaN layer contains 32 at.% of Ga and 26 at.% of N as well as 27 at.% of C and 15% at.% of O. The detected C element is mainly derived from the unreacted precursor, while the Ga-O impurity is ascribed to the residual oxygen in the chamber.

Table 1 Hall measurements of PEALD-grown GaN films on glass substrate.

Cycles	Thickness (nm)	Resistivity (Ω cm)	Mobility (cm^2/Vs)	Carrier density (cm^{-3})
50	4.8	4.1	0.4	8.5×10^{13}
100	9.3	1.6	1.0	3.2×10^{14}
200	19.3	1.1	3.3	5.5×10^{15}

The electrical properties of the GaN thin films, 50 (~5 nm), 100 (~9 nm) and 200 (~19 nm) PEALD cycles of GaN thin films on glass substrates, such as their resistivity, mobility, and carrier density were determined from Hall effect measurements, as presented in Table 1. The room temperature Hall measurements reveal n-type conductivity for all the samples. Besides, the GaN film thickness has some effects on Hall mobility, that is, the 19 nm-thick GaN film shows a higher mobility ($3.3 \text{ cm}^2\text{V}^{-1}\text{s}^{-1}$) than that of the 4 nm-thick GaN film ($0.4 \text{ cm}^2\text{V}^{-1}\text{s}^{-1}$).

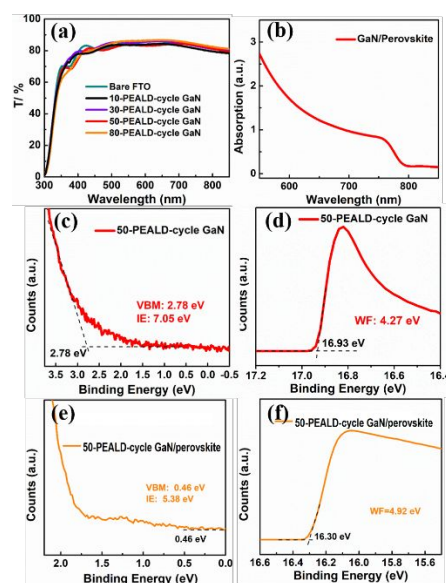


Fig. 4 (a) UV-vis transmittance spectra from FTO substrates coated with GaN of different thicknesses; (b) UV-vis absorption spectra from the GaN/perovskite films. UPS spectra for: (c, d) 50-PEALD-cycle GaN films; (e, f) perovskite films on top of the GaN film.

As-prepared GaN films as the ETL on the FTO substrates are fabricated into planar PSCs, which thickness is in the range between 10 and 80 PEALD cycles. The transmittance spectra shown in Fig. 4a clearly indicate that the transparency of the FTO glass is only minimally affected by the deposited GaN layer, a desirable result for

solar cell application. A $\text{FA}_{0.85}\text{MA}_{0.15}\text{Pb}(\text{I}_{0.85}\text{Br}_{0.15})_3$ perovskite absorber layer is subsequently deposited on top of the GaN films via the one-step spin-coating method described in the Experimental Section. The wettability of the perovskite precursor to the GaN layers is evaluated using contact angle measurements (Fig. S4), and contact angles between the perovskite solvents (DMF, DMSO) and the GaN layers were found to be less than 50° . A bandgap of 1.55 eV was calculated for the perovskite layer based on the absorption edge at 794 nm in the UV-vis absorption spectra (Fig. 4b).

It is well known that the energy level alignment between the GaN and perovskite layers is crucial for charge extraction and recombination in PSCs. Here, ultraviolet photoelectron spectroscopy (UPS) was employed to estimate the valence band minimum (VBM) and work function (ϕ) values of the 50-PEALD-cycle GaN and perovskite films, as shown in Fig. 4c-f. Fig. 4c and d show the UPS spectra (for the Fermi edge and secondary electron cut-off, respectively), from which an ionization energy (IE) of 7.05 eV and a ϕ of 4.27 eV were measured. A CBM value of 3.34 eV is further calculated based on the band-gap of 3.71 eV, also confirming that the as-prepared GaN film is n-type. Similarly, from UPS spectra of the sample after perovskite deposition in Fig. 4e and f, it can also be inferred that the perovskite film is a p-type semiconductor with a CBM of 3.83 eV. This film is similar to the perovskite film grown on TiO_2 in our previous report.⁴⁰ By combining the CBM, VBM and ϕ results of the p-type perovskite and n-type GaN, a p-n heterojunction model for the perovskite/GaN interface can be suggested.

PSC devices are further assembled by incorporating spiro-OMeTAD and Au electrodes. Unexpectedly, a 0.59 eV CBM mismatch is found at the interface of the GaN and perovskite layers in that case, which is usually considered unfavourable for device performance. In our cases, however, this energy-level mismatch does not seem to cause a severe deterioration in the cell performance, as will be shown in the next section.

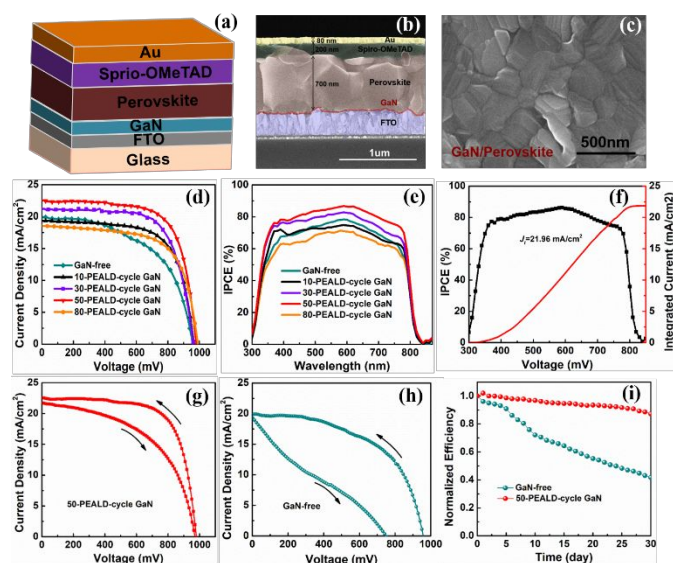


Fig. 5 (a) Schematic diagram and (b) cross-sectional SEM image of our GaN-based perovskite solar cell; (c) top-view SEM image of the

perovskite film grown on FTO/GaN; (d) J-V plots (reverse scan) and (e) IPCE spectra for the perovskite solar cells with GaN films of various thicknesses; (f) IPCE spectrum and integrated current curve of the best-performance cell; (g) and (h) J-V plots with forward and reverse scanning traces at scan rates of 10 mV/s and the voltage range from 0 to 1100 mV; (i) long-term stability test for the GaN-free and the best-performance devices.

Planar PSCs using GaN as ETL are fabricated by following a FTO/GaN/perovskite/spiro-OMeTAD/Au structure, as shown schematically in Fig. 5a. According to the cross-sectional SEM image in Fig. 5b, a ~ 700 nm-thick perovskite layer is coated on the FTO/GaN surface, followed by 200 nm-thick spiro-OMeTAD layer and 80 nm-thick Au electrode. From the top-view SEM image shown in Fig. 5c, it can be assessed that the perovskite layer deposited on the FTO/GaN surface is pin-hole free with an average grain size of ~ 300 nm. Good crystallinity of the perovskite film grown on GaN is crucial for high-efficient PSCs could be obtained in our device. The effect of GaN thickness on the quality of perovskite films has been studied by comparing the top-view SEM images of the perovskite films grown on bare-FTO as well as 10, 30, 50 and 80 PEALD cycles of GaN layers, respectively. As shown in Fig. S5, it can be clearly observed that the perovskite films grown on 10-80 PEALD cycles of GaN layers present flatter surface and larger perovskite grains than that grown on bare-FTO surface, suggesting that the introduction of GaN layer improves the quality of perovskite films. However, there is no macroscopic difference can be distinguished for the perovskite films grown on the different GaN layers.

The photovoltaic performance of the PSCs is characterized via J-V measurements under AM 1.5G illumination, as summarized in Fig. 5d and Table 2, respectively, and backward scanning curves (from forward bias to short circuit) are adopted. As a reference, a device without any GaN layer (GaN-free PSC) is also prepared, its efficiency is 10.38% with J_{sc} of 19.91 mA/cm^2 , V_{oc} of 952 mV, and FF of 0.548. The low performance is mainly ascribed to the serious charge recombination in the perovskite film due to poor electron extraction capacity. After a 10-PEALD-cycle GaN layer is introduced, the cell performance is improved with similar J_{sc} and V_{oc} but a significantly enhanced FF (0.656) compared to that of the reference device. Upon increasing the GaN film thickness increasing from 10 to 50 PEALD cycles, both J_{sc} and FF are clearly improved, and the 50-PEALD-cycle GaN-based device presents an efficiency of 15.18%, with J_{sc} of 22.56 mA/cm^2 , V_{oc} of 977 mV and FF of 0.689. However, further increasing the GaN film thickness (to 80 cycles) will lead to obvious reduction in the J_{sc} and FF , thus leads to a lower efficiency (11.42%). Therefore, too thick GaN layer is not beneficial to carrier transportation. As a contrast, the TiO_2 ETL-based PSC that with the same configuration was also prepared using our previous method.⁴⁰ Perovskite film on TiO_2 layer shows similar morphology with that on GaN layer (Fig. S6a). From Fig. S6b, the TiO_2 ETL-based PSC obtains a higher efficiency of 19.52% than the GaN ETL-based PSC, due to higher V_{oc} and FF . Besides, the intensity of incident photon-to-current conversion efficiency (IPCE) spectrum in the whole wavelength range increases with the GaN thickness increasing up to 50 PEALD cycles, indicating more efficient photo-responses and electron collection when increasing the GaN thickness, but reduces

for the 80-PEALD-cycle GaN-based device (consistent with the J - V results), as shown in Fig. 5e. Fig. 5f depicts the integrated current (J) of 21.96 mA/cm² for the 50-PEALD-cycle GaN-based cell, close to the corresponding J_{sc} value (22.56 mA/cm²). Fig. S7 gives the statistic results of the GaN-free and 50-PEALD-cycle GaN-based devices, which average efficiencies are 10.12% and 14.92%, respectively. Meanwhile, the narrow distribution of the device efficiencies reflects good reproducibility.

Table 2 J - V parameters of the PSCs (reverse bias scan)

Samples	J_{sc} (mA/cm ²)	V_{oc} (mV)	FF	Efficiency (%)
GaN-free	19.91	952	0.548	10.38
10-PEALD-cycle GaN	19.34	971	0.656	12.32
30-PEALD-cycle GaN	21.01	967	0.682	13.86
50-PEALD-cycle GaN	22.56	977	0.689	15.18
80-PEALD-cycle GaN	18.42	978	0.634	11.42

Possible hysteresis effects are also studied by comparing the J - V curves measured in both forward and backward directions for the reference device (Fig. 5h) and the 50-PEALD-cycle GaN-based cell (Fig. 5g). For the reference device, a large hysteresis is observed between the forward and reverse scans forward efficiency (4.38% vs 10.38%), whereas hysteresis was significantly reduced for the 50-PEALD-cycle GaN ETL-based device (11.87% vs. 15.18%), as shown in Fig. 5h. It is generally believed that the most common reason to this hysteresis in the J - V curve may be halide ion migration, interfacial defects or unbalanced charge extraction.⁴¹ It appears that the properties of the perovskite/GaN interface in our cells play an important role on that hysteresis behavior. Relatively low electron mobility in the as-prepared GaN layer may result in charge accumulation at the GaN/perovskite interface, which is supposed to be partly responsible for this hysteresis in the PSCs. Obviously, further improving the electron mobility of our PEALD-GaN layer as well as the properties of GaN/perovskite interface will be explored in our future work in order to minimize these effects. We also evaluate the ambient stability of the non-encapsulated 50-PEALD-cycle GaN-based PSC, which were stored in the dark at ambient conditions (25°C and ~40 RH%). The cell was tested each day for 30 days. As shown in Fig. 5i, the 50-PEALD-cycle GaN-based PSC can maintain 89% of its initial efficiency after 30-days storage, clearly superior to the GaN-free PSC. Moreover, to check the long-term light and temperature stability, both the GaN-free and 50-PEALD-cycle GaN-based PSCs were placed at 65°C and ~30 RH% in nitrogen atmosphere without any encapsulation, and tested at the maximum power point under continuous AM1.5G illumination over 80 h. The evolution of normalized efficiency values during the test is depicted in Fig. S8. The efficiency of the GaN-free device decreases to 29% of its initial value after 80 h because of the decrease of both J_{sc} and V_{oc} . However, a gentle degradation of efficiency for the 50-PEALD-cycle GaN-based device can be seen, and the device maintains 92% of its initial efficiency. According to previous reports, the potential reasons for this degradation include photo-activated defects and band alignment variation upon illumination, which lead to charge accumulation and recombination at the FTO/perovskite interface.⁴² Therefore, we speculate that the introduction of GaN layer

facilitates faster charge extraction and reduced interface recombination, thus leads to better stability.

Fig. 6 schematically shows the energy-levels diagram of the 50-PEALD-cycle GaN-based PSCs, and CBM mismatch of 0.59 eV at the GaN/perovskite interface can be clearly seen. In general, well-matched energy levels can boost electron extraction and reduce recombination. However, Minemoto et al thought that the optimum CBM position of the buffer or blocking layer was 0.0~0.3 eV higher than that of the perovskite layer, taking into account of the interface recombination.⁴³ Kuang et. al reported that a CBM mismatch of 0.69 eV at SnO₂/perovskite interface does not cause a severe deterioration to the cell performance.⁴² As the tunneling strongly depends on tunneling-layer thickness, in our case, electron tunneling is supposed to occur in the ~5 nm-thick GaN layer according to previous work on PbI₂ or insulating tunneling contacts in PSCs.⁴⁴⁻⁴⁶ Consequently, the degraded efficiency for our 80-PEALD-cycle GaN-based PSC could be ascribed to the fact that the increased GaN layer thickness reduces electron tunneling rate.

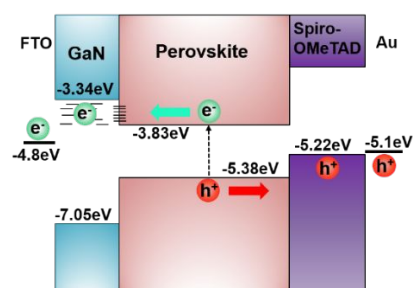


Fig. 6 Energy-levels diagram of the layers in 50-PEALD-cycle GaN-based PSCs

To further investigate the influence of the GaN layer on the cell performance, the steady-state photoluminescence (PL) spectra of the FTO/perovskite and FTO/GaN/perovskite systems were measured. As shown in Fig. 7a, the PL intensity was significantly quenched after inserting the 50-PEALD-cycle GaN layer between FTO and perovskite, indicating that the GaN layer can facilitate electron extraction effectively. The electron transport dynamics at the GaN/perovskite interfaces is further investigated by time-resolved PL, as shown in Fig. 7b. The average PL lifetime (τ) is estimated by fitting the curve with double-exponential function, relevant fitting parameters are listed in Table S1. In general, shorter PL lifetimes can be attributed to better electron extraction at the ETL/perovskite interface. Indeed, when the 50-PEALD-cycle GaN layer is introduced between FTO and perovskite, the PL lifetime decreases from 47 to 21 ns. In addition, electrochemical impedance spectra (EIS) measurement helped us understand the charge transport and recombination properties of the PSCs with and without the GaN layer. Fig. 7c shows the Nyquist plots in the dark at 0.8 V, and the fitting results derived from the equivalent circuit model are summarized in Table S2. Similar series resistance (R_s) values of ~22 Ω for both the devices are evaluated from the high frequency intercept on the x-axis, indicating the 50-PEALD-cycle GaN layer has negligible effect on the contact resistance. The arc at high frequency area represents the charge transport resistance (R_{ct}) at the FTO/perovskite or GaN/perovskite interface. Based on the

fitting results, the R_{ct} value of the GaN-based device (82.6 k Ω) is slightly decreased comparing to the GaN-free device (87.5 k Ω), reflecting an improvement of carrier transport to some extent. The other arc at low frequency region corresponds to the charge recombination resistance (R_{rec}). The 50-PEALD-cycle GaN layer results in an increase of R_{rec} value from 137.5 to 169.1 k Ω , which indicates that the GaN layer can restrain the recombination at the FTO/perovskite interface.

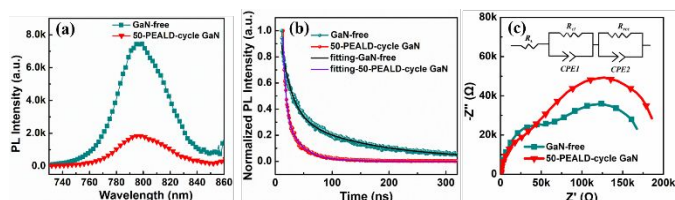


Fig. 7 (a) steady-state and (b) time-resolved PL spectra for the ETL-free (blue traces) and 50-PEALD-cycle GaN films; (c) Nyquist plots in the dark at 0.8 V. The frequency range is 0.1-10⁵ Hz. (c, inset): Equivalent circuit model. R_s , series resistance; R_{ct} , charge transport resistance; R_{rec} , recombination resistance; $CPE1$ and $CPE2$, chemical capacitance.

Experimental

Reagents and materials. PbI₂ (99.9985%), PbBr₂ (99.9985%), 4-*tert*-butylpyridine (TBP) and bis(trifluoromethane) sulfonimide lithium salt (LiTFSI) were obtained from Sigma-Aldrich. *N,N*-dimethylformamide (DMF), dimethylsulfoxide (DMSO) and chlorobenzene were purchased from Alfa Aesar. Methylammonium bromide (MABr), methylammonium iodide (MAI) and formamidinium iodide (FAI) were purchased from Shanghai Materwin New Materials Co., Ltd. Spiro-OMeTAD was purchased from Luminescence Technology Corp, and triethylgallium (TEG) (99.9999%) was acquired from Nanjing Aimouyuan Scientific equipment Co., Ltd. All these chemicals were used directly, without further purification. Laser-patterned FTO glass (Pilkington, 2.2 mm thick, sheet resistance = 15 Ω sq⁻¹) was sequentially cleaned with a mild detergent, distilled water and ethanol in an ultrasonic bath, and finally dried under a nitrogen stream.

Deposition of GaN thin films. GaN thin films were deposited on FTO glass substrates using an Angstrom-dep III PEALD reactor (Thin Film Technologies Ltd., of USA), equipped with an inductively coupled remote plasma (ICP) source. TEG as Ga the precursor, and a high-purity Ar/N₂/H₂ (1:3:6, 99.999%) plasma as the nitrogen source; high-purity Ar gas (99.999%) was used as the carrier gas for the precursor. The flow rates of both the carrier gas and the gas used in the plasma were set at 5 sccm, and the radio-frequency (RF) power and plasma frequency were 60 W and 13.56 MHz, respectively. Cleaned FTO glass substrates were put on the reactor chuck in the PEALD system and pumped down to the system base pressure of ~0.15 Torr, then the substrate chuck was heated to the growth temperature and let to equilibrate for 20 min. Initially, 5 plasma cycles were run to remove any residual oxygen from the surface. An ALD-GaN cycle consisted of a plasma exposure for 30 s and a purge of 30 s, followed by a TEG dose of 0.5 s and a reaction time of 45 s, and then a purge of 30 s. As indicated, for one ALD-GaN cycle, the

exposure times used for TEG and plasma were set at 0.5 s and 30 s, respectively, and pumping gas times of 30 s were required in between for purging the excess TEG and H₂O. A growth rate per cycle (GPC) of ~1.0 Å was determined by in situ spectroscopic ellipsometry (SE) for the thin films grown on FTO glass at 280°C. Compact GaN layers with various thicknesses (10, 30, 50 and 80 PEALD cycles) were used to fabricate planar PSCs devices.

Cell Fabrication. The fabrication method used for the PSCs was very similar to that reported in our previous work.⁴⁰ Specifically, a FA_{0.85}MA_{0.15}Pb(I_{0.85}Br_{0.15})₃ perovskite light absorber was deposited on the top of the GaN film by using a perovskite precursor solution prepared by mixing different molar quantities of 1.32 M PbI₂, 0.12 M PbBr₂, 1.08 M FAI, 0.24 M MAI and 0.12 M MABr solutions in 1L the solvent of a 4:1 volume ratio of DMF and DMSO. The perovskite films were fabricated by one-step anti-solvent method, that is, the perovskite precursor solution was dropped onto the GaN layer and spin-coated at 1000 rpm for 10 s and 5000 rpm for 30 s; 150 μ L of a chlorobenzene solution was dripped onto the spinning substrate at 15 s during the high speed step. The as-prepared films were heated at 150°C in a N₂ atmosphere for 10 min and then at 100°C in vacuum for 40 min. 200 nm-thick Spiro-OMeTAD layer was spin coated onto the top of the perovskite film at a speed of 3000 rpm, then heated at 60°C for 5 min. The perovskite film fabrication process was in the glovebox. Finally, an Au electrode about 80 nm thickness was deposited by thermal evaporation under a vacuum of 10⁻⁷ Torr.

Characterizations. Atomic force microscopy (AFM) measurements were carried out using a Bruker Dimension Icon instrument. Scanning electron microscopy (SEM) images were obtained using a Hitachi S-4800 SEM. Absorption and transmittance spectra were measured using a UV-vis spectrophotometer (UV-2550, Shimadzu) that covers wavelengths ranging from 300 nm to 850 nm. X-ray diffraction (XRD) measurements for the GaN films were carried out using a Smartlab GIXRD. X-ray photoelectron spectroscopy (XPS) data was acquired by using Thermo escalab 250Xi instrument. Contact angles were measured by using an OCA25, DataPhysics instrument. Hall measurements were performed by using an Phys Tech RH 2030 system at room temperature, under a DC magnetic field of 0.39 T. The valance band (VB) spectra were measured with a monochromatic He I light source (21.2 eV) and a VG Scienta R4000 analyser. A sample bias of -10 V was applied to observe the secondary electron cut-offs (SEC). The work functions (ϕ) were determined from the difference between the photon energy and the binding energy of the secondary cutoff edge. Current-voltage (J - V) curves were measured under AM 1.5 simulated sunlight (100 mW/cm²) from a Zolix SS150A lamp that was calibrated with a standard silicon reference cell, and recorded by a digital source meter (Keithley model 2602). The solar cells were masked with a black aperture to define the active area of 0.1 cm², and the J - V curves were measured during a forward bias scan going from -0.05 to 1.1 V and a reverse scan from 1.1 to -0.05 V at a scan rate of 30 mV/s. Incident photon-to-electron conversion efficiencies (IPCE) were measured using a lab-made setup with wavelength ranging from 350 nm to 850 nm. Steady-state photoluminescence (PL) spectra were measured using a PL spectrometer (Edinburgh

Instruments, FLS 900) with a xenon as the excitation source. The transient PL spectra were measured with the same instrument together with a pulsed diode laser (EPL-445, 0.8 $\mu\text{W}/\text{cm}^2$) run at a pulse frequency of 1 MHz. The electrochemical impedance spectra (EIS) were measured using a the Zahner IM6e electrochemical workstation in the dark in the frequency range from 0.1 to 10^6 Hz at a bias voltage of 0.8 V.

Conclusions

Low-temperature deposited GaN thin-films have been introduced into planar PSCs as ETLs for the first time. GaN thin-films are deposited on FTO glass substrate by PEALD at 280°C. This GaN film is compact and amorphous, which exhibits good transparency. Electron mobilities for the ~ 5 nm and ~ 19 nm-thick GaN layers on glass substrates are 0.4 and 3.3 $\text{cm}^2\text{V}^{-1}\text{s}^{-1}$, respectively. GaN layers with various thicknesses (10-80 PEALD cycles) are employed to fabricate planar PSCs. It is found that, even though a CBM mismatch of 0.59 eV exists at the n-GaN/p-perovskite interface, the 50-PEALD-cycle GaN-based cell can also exhibit 15.18% efficiency with less hysteresis, higher than the GaN-free device with 10.38% efficiency and severe hysteresis behavior. It is found that the GaN layer promotes the electron extraction at the FTO/perovskite interface and decreases charge recombination. Moreover, the GaN-based PSCs also display good long-term stability, demonstrating the feasibility and potential of GaN films as ETLs in planar PSCs. Further work to improve the GaN electronic mobility as well as to pattern GaN surfaces to improve the quality of perovskite films is underway.

Conflicts of interest

There are no conflicts to declare.

Acknowledgements

This work was supported by Beijing Natural Science Foundation (Grant No. 2184112), China Postdoctoral Science Foundation (Grant No. 2018M631333), State Key Laboratory of Advanced Metallurgy (Grant No. KF19-02), Fundamental Research Funds for the Central Universities (Grant No. FRF-TP-17-069A1), Natural Science Foundation of China (No. 51761145042, 51421002).

References

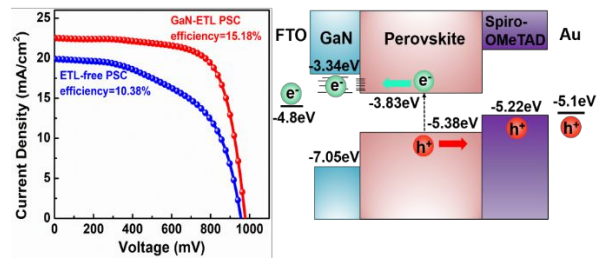
- 1 <https://www.nrel.gov/pv/cell-efficiency.html>
- 2 A. Kojima, K. Teshima, Y. Shirai, T. Miyasaka. *J. Am. Chem. Soc.*, 2009, **131**, 6050.
- 3 E. Avigad, L. Etgar. *ACS Energy Lett.*, 2018, **3**, 2240.
- 4 J. Liao, W. Wu, J. Zhong, Y. Jiang, L. Wang, D. Kuang. *J. Mater. Chem. A*, 2019, **7**, 9025.
- 5 D.-N. Jeong, D.-K. Lee, S. Seo, S.Y. Lim, Y. Zhang, H. Shin, H. Cheong, N.-G. Park. *ACS Energy Lett.*, 2019, **4**, 1189.
- 6 B. Yu, H. Zhang, J. Wu, Y. Li, H. Li, Y. Li, J. Shi, H. Wu, D. Li, Y. Luo, Q. Meng. *J. Mater. Chem. A*, 2018, **6**, 19810.
- 7 D. Kim, C. Muzzillo, J. Tong, A. Palmstrom, B. Larson, C. Choi, S. Harvey, S. Glynn, J. Whitaker, F. Zhang, Z. Li, H. Lu, M.F.A.M. van Hest, J. Berry, L. Mansfield, Y. Huang, Y. Yan, K. Zhu. *Joule*, 2019, **3**, 1734.
- 8 J. Shi, Y. Li, Y. Li, D. Li, Y. Luo, H. Wu, Q. Meng. *Joule*, 2018, **2**, 879.
- 9 J. Shi, H. Zhang, Y. Li, J.J. Jasieniak, Y. Li, H. Wu, Y. Luo, D. Li, Q. Meng. *Energy Environ. Sci.*, 2019, **11**, 1460.
- 10 Q. Jiang, Y. Zhao, X. Zhang, X. Yang, Y. Chen, Z. Chu, Q. Ye, X. Li, Z. Yin, J. You. *Nat. Photonics*, 2019, **13**, 460.
- 11 Z. Zhu, X. Zheng, Y. Bai, T. Zhang, Z. Wang, S. Xiao, S. Yang. *Phys. Chem. Chem. Phys.*, 2015, **17**, 18265.
- 12 E.J. Juarez-Perez, M. Mankel, T. Mayer, W. Jaegermann, I. Mora-Seró. *J. Phys. Chem. Lett.*, 2014, **5**, 680.
- 13 Y. Wang, Y. Yue, X. Yang, L. Han. *Adv. Energy Mater.*, 2018, **8**, 1800249.
- 14 W. Ke, G. Fang, Q. Liu, L. Xiong, P. Qin, H. Tao, J. Wang, H. Lei, B. Li, J. Wan, G. Yang, Y. Yan. *J. Am. Chem. Soc.*, 2015, **137**, 6730.
- 15 M.F.M. Noh, C.H. Teh, R. Daik, E.L. Lim, C.C. Yap, M.A. Ibrahim, N.A. Ludin, A.R.M. Yusoff, J. Jang, M.A.M. Teridi. *J. Mater. Chem. C*, 2018, **6**, 682.
- 16 Q. Jiang, L. Zhang, H. Wang, X. Yang, J. Meng, H. Liu, Z. Yin, J. Wu, X. Zhang, J. You. *Nat. Energy*, 2016, **2**, 16177.
- 17 D. Yang, X. Zhou, R. Yang, Z. Yang, W. Yu, X. Wang, C. Li, S. Liu, R.P.H. Energy Environ. Sci., 2016, **9**, 3071.
- 18 S. Zhang, W. Chen, S. Wu, R. Chen, Y. Huang, Z. Yang, J. Li, L. Han, W. Chen. *J. Mater. Chem. A*, 2019, **7**, 18603.
- 19 S.S. Mali, J.V. Patil, H. Arandiyani, C.K. Hong. *J. Mater. Chem. A*, 2019, **7**, 17516.
- 20 S.N. Mohammad, H. Morkoc. *Prog. Quant. Electr.*, 1996, **20**, 361.
- 21 J. Wu. *J. Appl. Phys.*, 2009, **106**, 011101.
- 22 G. Koblmüller, F. Wu, T. Mates, J.S. Speck. *Appl. Phys. Lett.*, 2007, **91**, 221905.
- 23 D.L. Rode, D.K. Gaskill. *Appl. Phys. Lett.*, 2005, **66**, 1972.
- 24 H. Zhou, J. Mei, M. Xue, Z. Song, H. Wang. *J. Phys. Chem. C*, 2017, **121**, 21541.
- 25 O. Ergen, S.M. Gilbert, T. Pham, S.J. Turner, M.T.Z. Tan, M.A. Worsley, A. Zettl. *Nat. Mater.*, 2017, **16**, 522.
- 26 S.A. Kukushkin, A.M. Mizerov, A.S. Grashchenko, A.V. Osipov, E.V. Nikitina, S.N. Timoshnev, A.D. Bouravlev, M.S. Sobolev. *Semiconductors*, 2019, **53**, 180.
- 27 G. Li, W. Wang, W. Yang, H. Wang. *Surf. Sci. Rep.*, 2015, **70**, 380.
- 28 M.B. Haider, M.F. Al-Kuhaili, S.M.A. Durrani, I. Bakhtiari. *J. Mater. Sci. Technol.*, 2013, **29**, 752.
- 29 Y. Zhao, F. Qin, Y. Bai, Z. Ju, Y. Zhao, X. Zhang, S. Li, D. Zhang, J. Bian, Y. Li. *Vacuum*, 2013, **92**, 77.
- 30 D.M.G. Leite, A.L.J. Pereira, L.F. da Silva, J.H. Dias da Silva. *Braz. J. Phys.*, 2006, **36**, 1678.
- 31 F. Zaera. *J. Phys. Chem. Lett.*, 2012, **3**, 1301.
- 32 H. Wei, P. Qiu, M. Peng, Q. Wu, S. Liu, Y. An, Y. He, Y. Song, X. Zheng. *Appl. Surf. Sci.*, 2019, **476**, 608.
- 33 M. Alevli, A. Haider, S. Kizir, S.A. Leghari, N. Biyikli. *J. Vac. Sci. Technol. A*, 2016, **34**, 041511.
- 34 C. Ozgit, I. Donmez, M. Alevli, N. Biyikli. *J. Vac. Sci. Technol. A*, 2013, **30**, 01A124.
- 35 H.-Y. Shih, M.-C. Lin, L.-Y. Chen, M.-J. Chen. *Nanotechnology*, 2015, **26**, 014002.
- 36 S. Liu, Y. He, H. Wei, P. Qiu, Y. Song, Y. An, A. Rehman, M. Peng, X. Zheng. *Chin. Phys. B*, 2019, **28**, 026801.
- 37 D.H. Kim, M.D. Losego, Q. Peng, G.N. Parsons. *Adv. Mater. Interf.*, 2016, **3**, 1600354.
- 38 O. Dakir, M. Houmad, A. Benyoussef, A.E. Kenz. *Optik*, 2017, **14**, 60.
- 39 Y. Chen, J. Liu, K. Liu, J. Si, Y. Ding, L. Li, T. Lv, J. Liu, L. Fu. *Mater. Sci. Eng. R*, 2019, **138**, 60.

ARTICLE

Journal Name

- 40 H. Zhang, J. Shi, L. Zhu, Y. Luo, D. Li, H. Wu, Q. Meng. *Nano Energy*, 2018, **43**, 383.
- 41 W. Tress, N. Marinova, T. Moehl, S.M. Zakeeruddin, M. K. Nazeeruddin, M. Grätzel. *Energy Environ. Sci.*, 2015, **8**, 995.
- 42 Y. Kuang, V. Zardetto, R. Gils, S. Karwal, D. Koushik, M.A. Verheijen, L.E. Black, C. Weijtens, S. Veenstra, R. Andriessen, W.M.M. Kessels, M. Creatore. *ACS Appl. Mater. Interfaces*, 2018, **10**, 30367.
- 43 T. Minemoto, M. Murata. *Sol. Energ. Mat. Sol. C.*, 2015, **133**, 8.
- 44 P. Zhao, B.J. Kim, H.S. Jung. *Mater. Today Energy*, 2018, **7**, 267.
- 45 Q. Wang, Q. Dong, T. Li, A. Gruverman, J. Huang. *Adv. Mater.*, 2016, **28**, 6734.
- 46 M.-C. Shih, S.-S. Li, C.-H. Hsieh, Y.-C. Wang, H.-D. Yang, Y.-P. Chiu, C.-S. Chang, C.-W. Chen. *Nano Lett.*, 2017, **17**, 1154.

Table of Contents



Plasma-enhanced atomic-layer-deposited GaN thin-films have been introduced into planar perovskite solar cells as electron transport layers.